Available online at www.sciencedirect.com

jmr&t Journal of Materials Research and Technology

www.jmrt.com.br

Original Article

Retained austenite phase detected by Mössbauer spectroscopy in ASTM A335 P91 steel submitted to continuous cooling cycles

Jorge I. Besoky[a], *Claudio A. Danon*[b], *Cinthia P. Ramos*[a,c,*]

[a] *Gerencia Investigación y Aplicaciones, Comisión Nacional de Energía Atómica, Av. Gral. Paz 1499, San Martín, Buenos Aires B1650KNA, Argentina*

[b] *Gerencia Materiales, Comisión Nacional de Energía Atómica, Av. Gral. Paz 1499, San Martín, Buenos Aires B1650KNA, Argentina*

[c] *CONICET, Buenos Aires, Argentina*

ARTICLE INFO

Article history:
Received 13 July 2018
Accepted 14 January 2019
Available online 19 February 2019

Keywords:
9% Cr steel
Martensitic transformation
Retained austenite
Mössbauer spectroscopy

ABSTRACT

Samples of ASTM A335 P91 steel submitted to continuous cooling at different rates were analyzed in the form of foils and powders by means of Mössbauer spectroscopy. The Continuous Cooling Transformation (CCT) diagram of steel ASTM A335 P91 displays two basic microstructural domains at low temperatures – ferritic and martensitic – whose limits depend on the austenite holding temperature, the precise chemical composition and the cooling conditions from the austenite mother phase. Under certain conditions, the martensitic transformation may not be completed, leading to a final microstructure with a non-negligible percentage of the austenite phase retained in a metastable state. This retained austenite could be detrimental for the mechanical properties of the steel.

Mössbauer analysis suggested that powdering process promotes the retained austenite transformation to martensite; in particular, in the present case, all the austenite transformed into martensite during powdering. Foil samples instead displayed retained austenite whose relative fraction was determined as a function of the cooling rate. At the same time, the carbon content of retained austenite was estimated for the faster cooled samples; a preliminary explanation for the observed trends is given.

1. Introduction

To increase the thermal efficiency and to reduce the environmental pollution from power generating plants (fossil fuel and nuclear systems), it is necessary to use increasingly high steam temperatures and pressures (in the order of 600 °C/30 MPa). These requirements have raised, over the last decades, a demand on materials with improved properties under those conditions. High Cr (9–12%) martensitic–ferritic steels exhibit good resistance to stress-corrosion cracking, higher thermal conductivity and lower thermal expansion coefficients as compared to austenitic stainless steels. Among the steels with high chromium content, an important group is the so-called modified 9Cr–1Mo. These steels are known

* *Corresponding author.*
E-mail: ciramos@cnea.gov.ar (C.P. Ramos).

https://doi.org/10.1016/j.jmrt.2019.01.005

as Grade 91 (T91 for tubing and P91 for piping) and their chemical composition design includes minor additions of niobium, vanadium and nitrogen. The high creep strength of P91 steels enables higher design stresses than those allowed by 2.25Cr–1Mo (P22) or X20 CrMoV 12 1 (12Cr–1Mo steel) up to 625 °C. Other properties of grade 91 steels are good oxidation resistance, resistance to hot hydrogen attack and adequate fracture toughness. In order to qualify as suitable materials, careful and precise manufacturing procedures are to be followed.

The main features of the Continuous Cooling Transformation (CCT) diagram of P91 steels have been already studied [1]. Depending on the austenitic grain size and the cooling rate, the final microstructure may be fully martensitic (if the cooling path only goes through the field outlined by M_s and M_f, which are the martensite start and finish temperatures, respectively [2]), fully ferritic or a mixed martensitic–ferritic one. There is also ample evidence of the presence of retained austenite (RA), not reported in the CCT diagrams, in the microstructure of these steels under different experimental or processing conditions [3–7]. In particular, and depending on the tempering temperature, RA could promote the generation of non-tempered or inhomogenously tempered martensite in steel components or parts, producing a negative influence in the mechanical properties of the material during its service life [8]. Even a low fraction of film like, interlath RA could affect the mechanical performance of some high Cr steels if a low-temperature tempering or pre-tempering – such as the one used in manufacturing steam turbine rotors [9] – is expected. As a matter of fact, RA has been shown to be stable as an interlath film for tempering temperatures of up to ~525 °C in standard P91 [4] and B-added 9–10%Cr [10,11] steels; from that value on, austenite has been observed to decompose to a film-like $M_{23}C_6$ carbide identified as responsible for tempering embrittlement [10,11]. Hence the importance of assessing the RA content after continuous cooling cycles.

Mössbauer spectroscopy is a high sensitivity technique which provides information on Fe alloys not accessible by other characterization tools such as X-ray diffraction or metallographic analysis [12]. It is particularly useful to distinguish the matrix component phases (martensite, ferrite) from the parent austenite phase in steels, because the former are ferromagnetic while the latter is paramagnetic at room temperature (RT). Thus, they exhibit distinctively characteristic hyperfine patterns, a singlet and/or a doublet for austenite [13] and a sextet for the ferromagnetic phases. The very low detection threshold of the technique allows revealing RA even in very small amounts when XRD measurements fail to detect it [14–16]. However, special care should be taken when preparing samples. There are basically two ways to prepare the samples in order to get a suitable Mössbauer absorber, i.e. the one which enables to obtain a well-defined spectrum in the shortest time; that is as powder or as a thin foil (always taking into account the thin absorber approximation [17]).

It has been reported that powdering in steels could promote martensitic transformation and, in case of a low fraction of RA, information about this phase could be lost. This effect was observed for example in a duplex steel UR45N, in which the difference in the relative abundance of the austenite between bulk (i.e., thin foils) and powder samples was about 25% on the average [18]. A similar transformation due to mechanical stresses was observed by Skrzypek et al. [19] in hard ball bearing steels.

There is previous literature related to the Mössbauer spectroscopy study of retained austenite in different alloys [20,21].

The aim of this work is then twofold; on one hand to show the importance of the Mössbauer absorber preparation to detect RA in low-carbon ferritic–martensitic ASTM A335 P91 steels and, on the other hand, to follow the trend of the RA phase fraction – and its estimated carbon content – as a function of the cooling rate in continuous cooling cycles applied to these steels.

This work is a sequel of a more detailed, previously conducted dilatometric, microscopic and structural analysis [22].

2. Material and methods

The samples were obtained from an ASTM A335 P91 seamless steel pipe of 219 mm external diameter and 32 mm wall thickness, initially normalized at 1050 °C during 20 min and then tempered at 780 °C during 40 min. The chemical composition of the examined steel is shown in Table 1.

Prismatic 25 × 5 × 5 mm samples were machined following the axial direction of the pipe and exposed to continuous cooling cycles, with different cooling rates, in an Adamel DHT 60 dilatometer. After austenization at 1050 °C for 30 min, the samples were cooled at 100, 115, 150 and 200 °C/h in order to make sure that the final microstructure falls into the mixed ferritic–martensitic domain of the CCT diagram. The cooling rates were selected based on our previous studies where the critical velocity for ferrite formation had been bounded to a range between 100 and 60 °C/h and the critical velocity for martensite formation to a range between 200 and 150 °C/h.

With the aim of performing a thorough characterization, Mössbauer spectroscopy was complemented with Field Emission Gun Scanning Electron Microscopy (FEG-SEM) observations and X-ray Diffraction (XRD) analysis.

Micrographs were obtained with a scanning electron microscope Carl Zeiss NTS, SUPRA 40.

XRD measurements were done in a Panalytical Empyrean diffractometer, using the θ–2θ Bragg-Brentano geometry, a flat graphite monochromator and Ni-filtered Cu-Kα radiation. The

Table 1 – Main alloying elements of the ASTM A335 P91 steel (wt.%).

C	Mn	Si	Cr	Mo	V	Nb	N	Ti	P	S	Ni
0.100	0.360	0.240	8.370	0.880	0.211	0.075	0.061	0.004	0.014	0.001	0.15

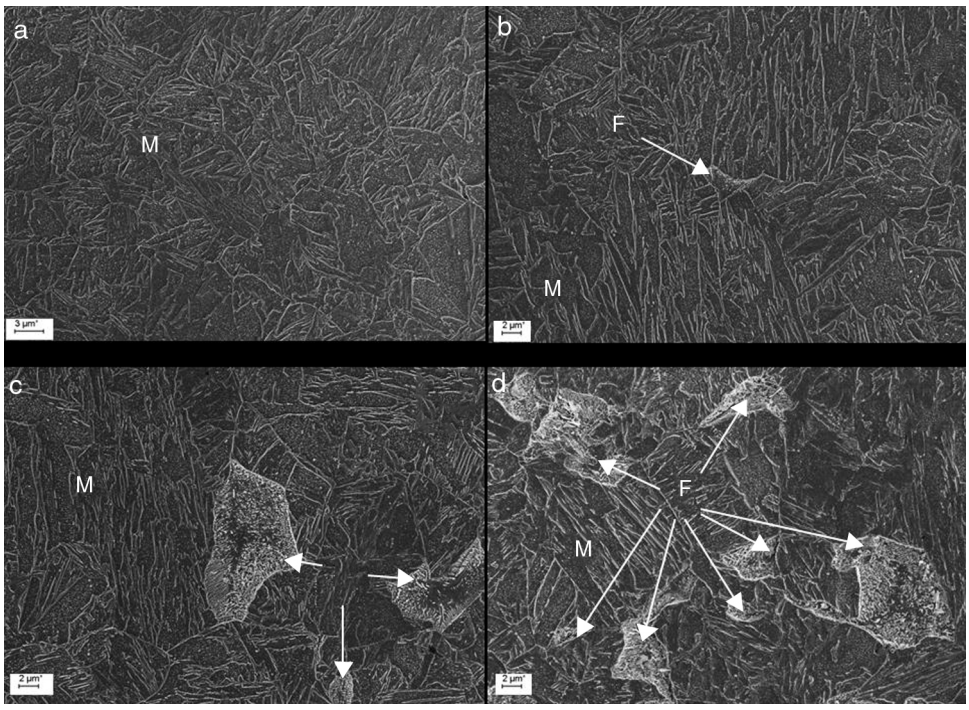

Fig. 1 – FEG-SEM images of the samples cooled at 200 °C/h (a), 150 °C/h (b), 115 °C/h (c) and 100 °C/h (d). M: martensite, F: ferrite.

diffracted radiation was collected between 35° and 120° (2θ) with an ultra-fast PixCel area detector. The step scan angle and step scan time were settled in 0.026° and 939 s respectively. The spectra were processed by the Rietveld refinement method [23] using the software MAUD (Materials Analysis Using Diffraction) [24].

Mössbauer absorbers were prepared in two ways: as powders obtained with a diamond file and as foils mechanically thinned with SiC abrasive grinding papers to a final thickness of about 100 μm; this task was carried out very carefully to avoid heating or any kind of transformation. Measurements were performed in transmission geometry with a ^{57}Co source in a Rh matrix. Spectra were collected at room temperature (RT), run at 10 mm/s and then fitted using the WinNormos least-squares program [25].

The relative fractions of particular phases to the spectra were determined assuming the same recoilless fractions for all of them, even if it is known that there is a difference between the Debye temperatures of austenite and the matrix components (martensite and ferrite) of about 2%. The consequence of neglecting this difference is an overestimation of the RA content of only 0.1% [14,15].

3. Results

3.1. FEG-SEM observations

In Fig. 1a a FEG-SEM micrograph corresponding to the sample cooled at 200 °C/h shows a lath martensitic microstructure with carbides of different size and morphology. In Fig. 1b, for the sample cooled at 150 °C/h, also a lath martensitic microstructure is seen but small ferrite nodules begin to show up, although in scarce content. In the micrographs of samples cooled at 115 °C/h and 100 °C/h (Fig. 1c and d), two zones can be distinguished: a martensitic one with wider laths than those observed for the samples cooled at higher rates, and a ferritic one with numerous precipitates inside exhibiting different size and morphology. This analysis allows confirming the information given in the CCT diagram of this kind of steels; when the cooling rate decreases, the microstructure evolves from fully martensitic to a mixed ferritic-martensitic one. The micrographs clearly show this evolution displaying an increasing ferrite fraction in lowering the cooling rate.

3.2. XRD analysis

In the Rietveld analysis of the XRD patterns (Fig. 2), the diffraction peaks of the phases composing the matrix (martensite and ferrite) were completely overlapped. However, by using the supporting evidence from FEG-SEM observations and the fact that these phases display a significant difference as for peak breadths, they could be modeled and deconvoluted. On the other hand, the main peak of austenite detected in the samples cooled at 200 and 150 °C/h is wide and has low intensity, very likely because of the small size of the diffraction domains and/or as a consequence of microstress–microstrain effects in the samples. This fact inhibits from an accurate estimation of the RA content; any calculation could give an appreciable error.

3.3. Mössbauer spectra analysis

3.3.1. Influence of the absorber preparation on the observed spectra

As already introduced, the two preparation ways for the absorbers were tested. In Fig. 3 a comparison between powder

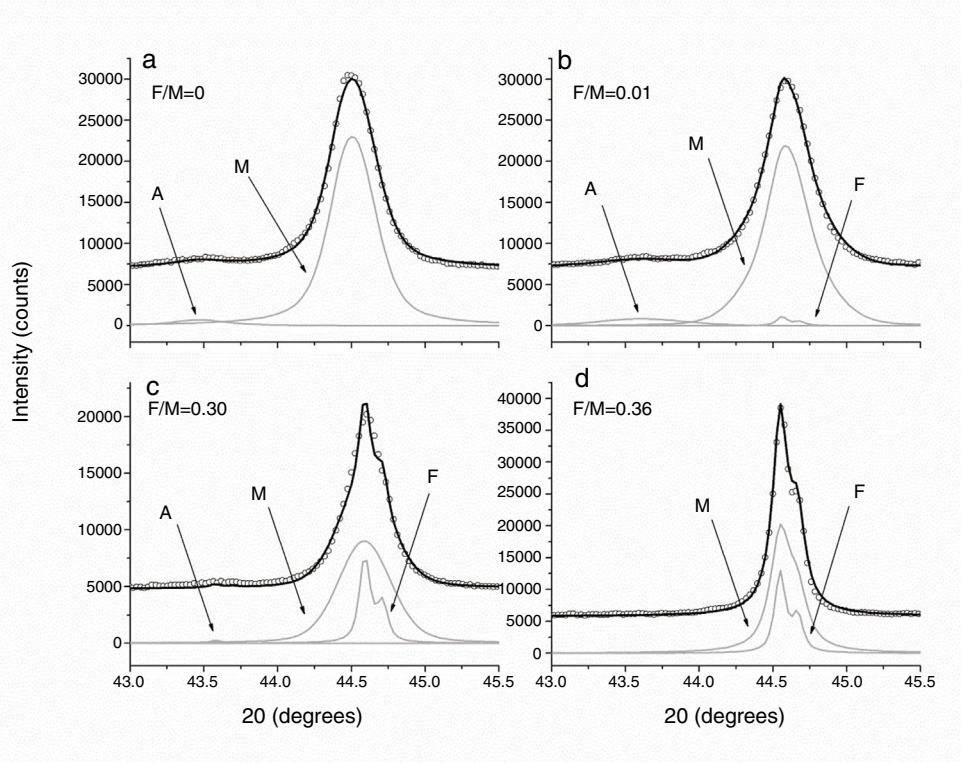

Fig. 2 – XRD main peaks for the patterns of the samples cooled at 200 °C/h (a), 150 °C/h (b), 115 °C/h (c) and 100 °C/h (d). M: martensite (101) and (110), F: ferrite (110), RA: retained austenite (111), F/M: ferrite/martensite fraction obtained from XRD pattern fittings.

and thin film absorbers can be seen. It is evident that in the powdered samples information about the RA presence is totally lost. In contrast, for the foil samples a paramagnetic contribution is clearly distinguished in the center of the spectra, even in the sample cooled at 100 °C/h in which no RA had been detected by XRD analysis.

3.3.2. *Fitting details*

Fitting of the spectra corresponding to the thin foils was made based on our previous work in a T91 steel submitted to a tempering process at 780 °C during different time intervals [26]. The matrix phases were modeled with five sextets; this number of subspectra was proposed in order to account for the influence of Cr in the hyperfine magnetic field, as the main substitutional atom. A sixth sextet was also added in all of the spectra coming from a small contribution at low fields denoting the presence of carbides of the cementite type.

In this way, a singlet and/or doublet pattern was used to account for the paramagnetic phase (RA) and six sextet patterns for the magnetically ordered phases (matrix: ferrite and/or martensite and precipitated carbides). Unfortunately, a distinction between ferrite and martensite is not possible by means of Mössbauer spectroscopy when analyzing low-carbon content alloys [27].

The subspectra for the matrix phases displayed isomer shifts (IS) and quadrupole shifts ($2\varepsilon Q$) near 0.0 mm/s in all cases, as expected from the fact that these values are zero for metallic iron (αFe) [28].

As a representative example, Fig. 4 displays the fitted Mössbauer spectrum of the sample cooled at 150 °C/h. The main magnetic component corresponding to the matrix phases arises from Fe atoms with no Cr atoms as nearest neighbors (magnetic hyperfine field $B_{hf} \sim 34.2$ T) meanwhile the other components ($B_{hf} \sim 31.4$, 29.3, 26.9, 24.5 T) are attributed to Fe atoms perturbed by one, two, three and four nearest neighbor Cr atoms, respectively. This is in accordance to the decreasing effect of a non-magnetic atom as Cr on the B_{hf} [29]. The sextet with $B_{hf} \sim 19.9$ T is representative of the precipitation of alloyed cementite $(Fe, Cr)_3C$ [30–32]. A doublet with QS ~ 0.25 mm/s and IS ~ −0.07 mm/s and a singlet with IS ~ −0.12 mm/s are indicative of the RA presence.

In the spectrum corresponding to the sample cooled at 200 °C/h the paramagnetic RA was also fitted to a singlet and a doublet but in the spectra of the samples cooled at 115 and 100 °C/h only a singlet was needed.

3.3.3. *Calculation of RA phase fraction*

Concerning the estimation of the amount of RA as a function of the continuous cooling rate, it is important to point out that the areas corresponding to each subspectrum in a Mössbauer spectrum are proportional to the relative abundance of each Fe environment present in the sample. Thus, the RA fraction is obtained from the singlet and/or doublet area in each spectrum (Table 2). Any contribution of precipitates other than cementite-type ones, which could add a minimal doublet subspectrum superimposed to those of RA, was dismissed. This fact taken into account, along with the small amount of RA in

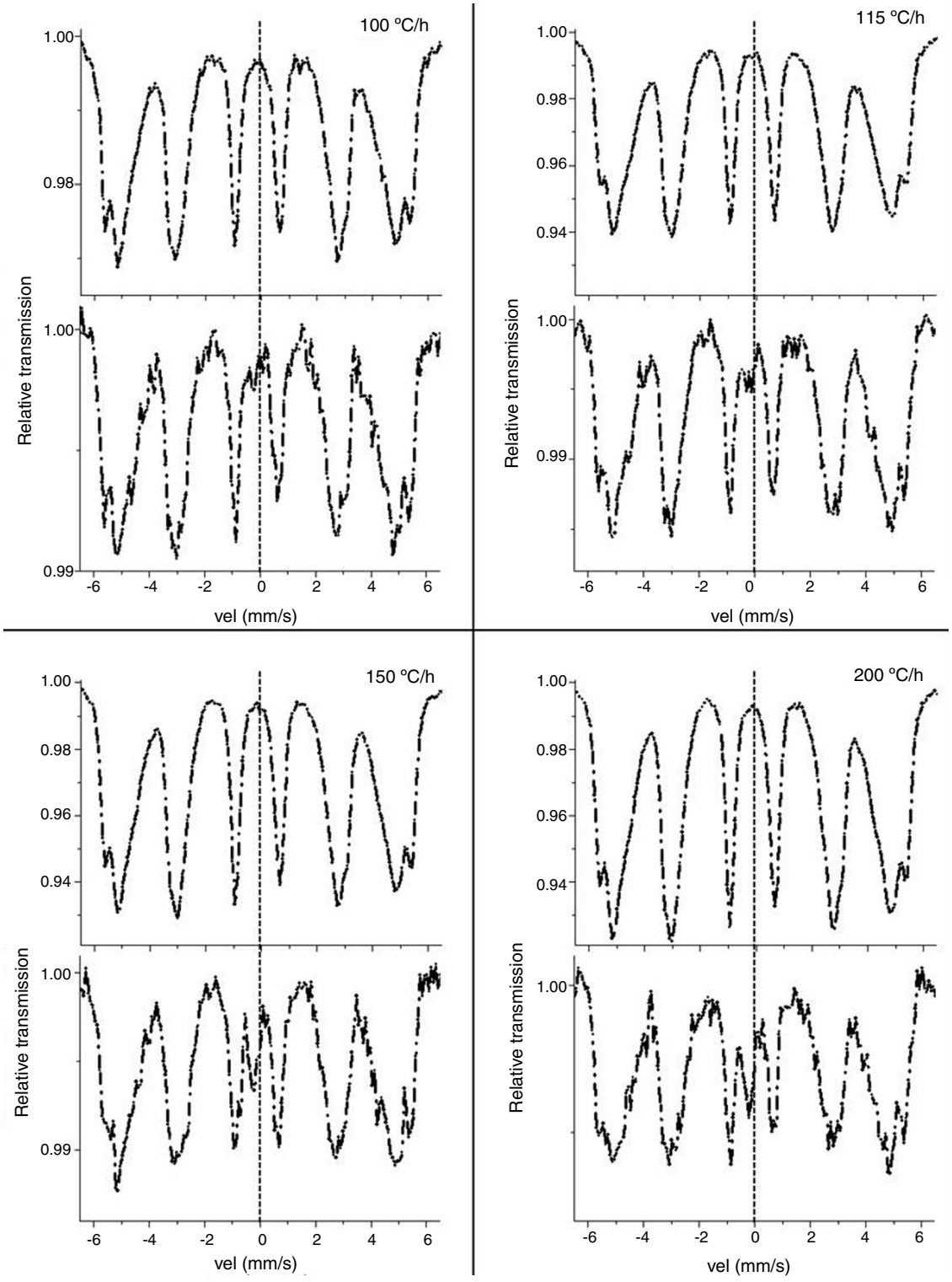

Fig. 3 – Mössbauer spectra for samples cooled at 100, 115, 150 and 200 °C/h. Powder samples (up) and foil samples (bottom). Dotted lines in zero velocity are a guide to the eye, in order to see the differences between powdered and foil samples. RA paramagnetic signals can be detected to the left of the dotted lines.

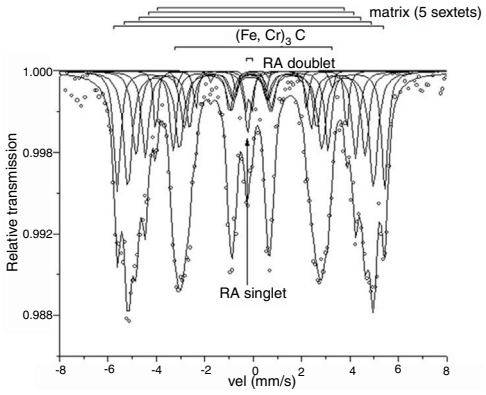

Fig. 4 – Fitted Mössbauer spectrum of the sample cooled at 150 °C/h. The five sextets representing the different Fe environments of the matrix phases, the sixth sextet characteristic of (Fe, Cr)$_3$C precipitates and the paramagnetic signals (singlet and doublet) corresponding to the RA are indicated.

some of the samples and its instability during sample preparation, the estimated fraction of RA should be understood from a qualitative point of view, giving a tendency, but not as definitive quantitative information.

3.4. M_s temperature

The dilatometric curves of all samples were analyzed in order to estimate the M_s transformation temperature in two ways: (1) by fitting the linear contraction of the austenite and evaluating the deviation from this behavior and (2) employing the offset method [33], assuming a 2% of the total volume contraction for the steel. In Table 3 the calculated values are compared.

Table 3 – Martensitic start transformation temperature (M_s) for the samples cooled at different rates.

Cooling rate (°C/h)	M_s (°C)	
	Linear best fit	Offset method
200	373	361
150	362	361
115	381	365
100	419	398

4. Discussion

4.1. Powdered vs. thin foil Mössbauer absorbers

At RT the martensitic phase is stable while the parent austenite phase is metastable. According to the previous literature, the plastic deformation induced by powdering of the sample would promote the transformation from austenite to martensite due to strain relaxation. In the foil sample instead the surrounding matrix would act as a barrier to inhibit strain relaxation [34,35]. The results here obtained from powdered samples effectively show that the powdering process triggers the martensitic transformation and all the RA turns into martensite.

Therefore, special care has to be taken while preparing powdered Mössbauer absorbers of some materials, because the phase composition or phase structure might change during powdering. In [18,36], for example, the authors compared the hyperfine parameters obtained from different steel samples prepared in the two ways (foil versus powder). In both of the works, the foil and the powder samples exhibited an amount of non-magnetic austenite phase. In our case, for the P91 steel submitted to different cooling rates, RA totally vanished in the powdered samples. These results let us conclude that for this kind of steels the right procedure to obtain the Mössbauer absorbers is as thin foils.

Moreover, due to residual stresses at the surface layer of the samples during thin foil preparation the RA fraction at the surface diminishes [37], so it is better to apply Mössbauer Spectroscopy in transmission mode to obtain information coming from the whole sample thickness.

4.2. Estimation of the carbon content in RA for the samples cooled at 200 and 150 °C/h

First of all it is worth noting that interstitial C prefers octahedral sites in the austenite structure, independently from the total C content in the alloy [38].

From the results here obtained by the Mössbauer spectra fitting corresponding to thin foil samples it is important to remind that Fe sites in austenite with no C near neighbors (nn) but with 0–4C atoms as next near neighbors (nnn) are usually represented by a paramagnetic singlet, whereas a quadrupole doublet represents Fe atoms in austenite having one C atom as nn on interstitial sites [13]. Due to coulombic repulsion [39] and size effects [40] of the C atoms, configurations representing Fe atoms with more than one C atom as nn are not expected. The fraction of Fe atoms with a C atom as nn can be described as $f = 6y$ [40], where y is the fraction of interstitial occupied sites. Furthermore, considering the Mössbauer spectra, the f fraction can also be calculated as the ratio of the doublet area to the whole austenite spectral area (singlet + doublet). Since in a fcc lattice there is one octahedral interstitial site per lattice point, in the case of the samples cooled at 150 and 200 °C/h – whose Mössbauer spectra reflect the presence of sites with one C atom as nn and 0–4C atoms as nnn,

Table 2 – RA content estimated from the relative areas of the paramagnetic components in the Mössbauer spectra of the studied samples.

Cooling rate (°C/h)	100	115	150	200
RA content (wt.%)	1.13 ± 0.18	1.86 ± **0.22**	3.89 ± **0.27**	5.47 ± **0.26**

Table 4 – Fraction of Fe atoms with a C atom as nearest neighbor (nn) and estimated wt.% C in retained austenite (RA) of the samples cooled at 150 and 200 °C/h (see text).

Cooling rate (°C/h)	*f*	*y*	C content in RA (wt.%)
200	0.25	0.042	0.91
150	0.29	0.048	1.02

i.e.,doublets ans singlets respectively – the C concentration in RA can be estimated, using the expression [13]:

$$\text{wt\%}\quad C\,(\text{in austenite}) = \frac{12.01y}{55.85 + 12.01y} * 100$$

Having in mind that the studied steel has a substantial Cr content, a random distribution of this element has also been taken into account to perform an estimation of the wt.% C content in RA for the cited samples (Table 4).

On the other hand, the C content of RA in samples cooled at the slower rates (115 and 100 °C/h) cannot be estimated by the same method. However, it is reasonably expected that RA will have a lower C concentration, taking into account that:

i. The nucleation and growth of a ferrite fraction during cooling will "scavenge" some C from the matrix, because C has a low solubility limit in ferrite and precipitates heavily from the early stages of ferrite nucleation.
ii. Some more C will be removed from the matrix because of carbide precipitation in martensite due to autotempering. This process could be favored by the increase of the M_s temperature that was effectively observed for these samples (see below).

The decreased global C content under slow cooling rate conditions is, of course, counterbalanced by the reduction of the RA volume fraction (see Table 2), even so indications of the decrease of the interstitial C content of non-transformed austenite have already been reported for isothermally treated 9%Cr steels [41].

Thus, according to these assumptions, the presence of only a paramagnetic singlet or a singlet plus a doublet in the Mössbauer spectrum could be associated to a RA phase having lower or higher C contents respectively. Direct measurements of the C content in RA by suitable techniques such as atom probe tomography or high resolution analytical transmission microscopy are needed to confirm this hypothesis.

4.3. M_s behavior

From Table 3 it can be seen that for the samples cooled at slower rates (115 and 100 °C/h), in which the content of ferrite phase is higher, M_s increases following the shape of the reported CCT diagram. This increase of the M_s value is, of course, in line with the reduction of the matrix C content associated to the already mentioned carbide precipitation in ferrite.

More generally, the influence of alloying elements on the M_s temperature can be obtained from empirically established equations [42]. The one that better accounts for our case is

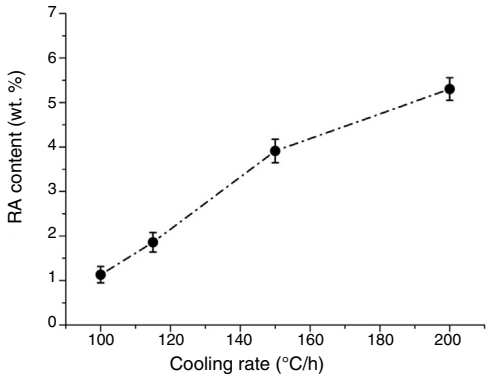

Fig. 5 – Influence of the cooling rate on the content of RA. The dotted line is a guide to the eye.

that of Finkler [43]:

$$M_s\,(^\circ C) = 635 - 474 * [(\%C) + 0.86\,(\%N) - 0.15\,(\%Nb + \%Zr) - 0.066\,(\%Ta + \%H_f)] - [17\,(\%Cr) + 33\,(\%Mn) + 21\,(\%Mo) + 17\,(\%Ni) + 39\,(\%V) + 11\,(\%W)] \quad (1)$$

which gives an M_s value of 384 °C for the steel composition here studied. This result agrees fairly well with the experimental obtained values (Table 3). Taking into account that Eq. (1) has been obtained as an empirical expression from a low-carbon steel database – and must be used cautiously for that reason – the high C content in RA estimated from Mössbauer calculations (~1 wt.% for samples cooled at 150 and 200 °C/h), would bring an estimated M_s temperature much lower than the experimentally found for the bulk of the matrix. This fact suggests that the high C content in these faster cooled samples plays a significant role in stabilizing the RA found at RT.

4.4. RA content and cooling rate: chemical vs. mechanical stability

As can be inferred from the results displayed in Table 2, the RA content increases for increasing cooling rates. In Fig. 5, results from Table 2 were plotted to appreciate them in more detail. The slope of the trend line is more pronounced for the slower cooling rates, up to 150 °C/h – cooling rate from which the microstructure tends to be completely martensitic – and from that value the increasing trend of the RA content becomes smoother.

The slight change of the slope in the RA content versus cooling rate plot shown in Fig. 5 could be interpreted as an indication that two types of effect play a role on the stability of RA in ASTM A335 P91 steels, namely, a chemical one referred to the C content in the RA and a mechanical one related to strains induced in the sample.

For the samples cooled at higher rates (200 and 150 °C/h) the analysis of the Mössbauer spectrum evidenced the presence of C as nnn and nn (singlet + doublet respectively), which allowed the estimation of a high C content in the RA. Thus, it can be said that the chemical effect would prevail over the mechanical one when RA is dispersed in a fully martensitic matrix

(for the sample cooled at 200 °C/h) or a quasi-fully martensitic matrix (for the sample cooled at 150 °C/h). It is interesting to point out that the phenomenon of inverse stabilization – or destabilization – of austenite has been observed in P91 steel specimens *isothermally* treated for increasing times at temperatures above M_s, before being transformed to martensite [7]. Destabilization was explained by the authors on the grounds of a purely chemical reasoning. Hence, according to that work, decreasing the time of permanence above M_s (i.e., increasing the cooling rate in the anisothermal case) would imply austenite stabilization.

For cooling rates below 150 °C/h, the strain induced in austenite by the nucleation and growth of ferrite could promote a more significant role for a mechanical factor. This effect, caused by the nature and volume fractions of the phases constituting the matrix in which the austenite grains are dispersed [34,35], adds to the chemical one. Specifically, plastic apparent transformation strains associated to the austenite to ferrite transformation have been measured for low C and interstitial free steels; the apparent transformation strain increases as the transformation proceeds *isothermally* at 750 °C [44]. In the same way, the study of lattice parameters of ferrite and austenite by in situ neutron diffraction allowed to conclude that tensile and compressive strains are actually developed in austenite and ferrite respectively during the course of the austenite-ferrite anisothermal transformation in a 0.2C–2Mn martensitic steel [45]. Under the present experimental conditions, slower cooling rates, allowing more time for precipitation, leave less C available to stabilize austenite; i.e. the significance of the chemical effect in this cooling rate range would be reduced. Thus, the reduction in the chemical stabilizing effect of C content and the simultaneous occurrence of mechanical strains due to partial transformation to ferrite that destabilize the non-transformed austenite would produce a more pronounced drop in the amount of RA by cooling at rates decreasing from 150 °C/h.

5. Conclusions

- Mössbauer spectroscopy is a more sensitive and accurate technique than XRD to detect small amounts of RA in ASTM A335 P91 steels submitted to continuous cooling in the 200–100 °C cooling rate range. The paramagnetic signals are well defined allowing a separation of the inner lines of the magnetic subspectra.
- RA is mechanically unstable and transforms completely to martensite when powdering bulk samples; for this reason Mössbauer spectroscopy absorbers should be prepared as thin foils.
- Cooling at different rates will likely produce different C contents in RA. The high C content estimated in RA by Mossbauer spectroscopy in the samples cooled at 200 and 150 °C/h is responsible for the significant decrease in M_s of the enriched austenite.
- A decrease in the RA volume fraction for decreasing cooling rate was observed. For the higher cooling rates, the stabilization of austenite could be attributed to the decrease of the permanence time above M_s. For the lower cooling rates, the stability of RA could be not only a consequence of a C enrichment provoking a decrease in M_s but it could also be related to austenite-ferrite transformation strain effects.

Conflicts of interest

The authors declare no conflicts of interest.

Acknowledgements

This work was supported by the Agencia Nacional de Promoción Científica y Tecnológica (ANPCyT), Ministerio de Ciencia, Tecnología e Innovación Productiva (MINCyT) [grant PICT 2014-2170].

REFERENCES

[1] Haarmann K, Vaillant JC. The T91/P91 book. 2nd. ed. Düsseldorf: Vallourec & Mannesmann Tubes; 2002.
[2] Bhadeshia HKDH. Martensite in steels. Mater Sci Metallur 2002. http://www.msm.cam.ac.uk/phase-trans/2002/martensite.html.
[3] Tsuchida Y, Tokuno K, Hashimoto K. Development and BOF manufacture of modified 9Cr–1Mo steel plates with excellent strength and toughness. Nippon Steel Tech Rep 1993;58(July):27–35.
[4] Hurtado-Noreña C, Danón CA, Luppo MI, Bruzzoni P. Evolution of minor phases in a 9PctCr steel: effect of tempering temperature and relation with hydrogen trapping. Metallur Mater Trans 2015;46A(9):3872–88.
[5] Shiue RK, Lan KC, Chen C. Toughness and austenite stability of modified 9Cr–1Mo welds after tempering. Mater Sci Eng 2000;A287(1):10–6.
[6] Mayr P, Palmer TA, Elmer JW. Specht direct observation of phase transformations in the simulated heat-affected zone of a 9Cr martensitic steel. Int J Mater Res 2008;99(4):1–6.
[7] Ning B, Liu Y, Shi Q, Gao Z, Yang L. Effects of austenite stabilization on the onset of martensite transformation in T91 steel. J Mater Sci Technol 2008;24(2):202–6.
[8] Bhadeshia HKDH. Honeycombe. Steels: microstructure and properties. 4th ed. Oxford: Butterworth-Heinemann; 2017.
[9] Mito Y, Miki K, Azuma T, Ishiguro T, Tamura O, Murata Y, et al. Effects of Cr and W content in high Cr ferritic heat-resistant steels on long-term creep rupture strength. In: Advances in materials technology for fossil power plants, Proceedings of the 7th international conference. 2013. p. 627–8.
[10] Fedorova I, Kostka A, Tkachev E, Belyakov A, Kaibyshev R. Tempering behavior of a low nitrogen boron-added 9%Cr steel. Mater Sci Eng A 2016;662:443–55.
[11] Dudova N, Mishnev R, Kaibyshev R. Effect of tempering on microstructure and mechanical properties of boron containing 10%Cr steel. ISIJ Int 2011;51:1912–8.
[12] Kuzmann E, Domonkos L, Kocsis M, Nagy S, Vertes A, Mehner H. Determination of retained austenite in steels alloyed with carbide formers. J Phys Coll 1979;40(C2):627–9.
[13] Tenuta Azevedo AL, Galvão da Silva E. Mössbauer study of retained austenite in a low C low alloy steel. Scripta Metallur 1978;12(2):113–7.
[14] Abe N, Schwartz LH. Quantitative Mössbauer effect spectroscopy — retained austenite in Fe–27 at.% Ni. Mater Sci Eng 1974;14:239–51.
[15] Ladriére JH, He XJ. Mössbauer study on retained austenite in an Fe–Mn–C dual-phase steel. Mater Sci Eng A 1986;77:133–8.

[16] Choi HJ, Schwartz LH. Fatigue crack propagation in intercritically tempered Fe–9Ni–0.1C and Fe–4Mn–0.15C. Metallur Trans A 1983;14:1089–99.
[17] Long GJ. The ideal Mössbauer effect absorber thickness. Mössbauer Effect Ref Data J 1983;8:42–9.
[18] Blachowski A, Ruebenbauer K, Jura J, Bonarsky JT, Baudin T, Penelle R. Mössbauer study of deformation induced martensitic phase transformation in duplex steel. Nukleonika 2003;48 Suppl. 1:S9–12.
[19] Skrzypek S, Kolawa E, Sawicki JA, Tyliszczac T. A study of the retained austenite phase transformation in low alloy steel using conversion electron Mössbauer spectroscopy and X-ray diffraction. Mater Sci Eng 1984;66(2):145–9.
[20] Krawczyk J, Bała P, Frąckowiak J. The Mössbauer spectroscopy studies of retained austenite. Arch Mater Sci Eng 2007;10(28):633–6.
[21] Bała P, Krawczyk J, Hanc A. Mössbauer spectroscopic investigation of retained austenite content of high-carbon tool steel during isothermal tempering of as-quenched samples. In: Proceedings of the International Symposium on the Industrial Applications of the Mössbauer Effect (ISIAME 2008), vol. 22. 2008. p. 205–10.
[22] Carrizo DA, Besoky JI, Luppo M, Danon CA, Ramos CP. Characterization of an ASTM A335 P91 ferritic-martensitic steel after continuous cooling cycles at moderate rates. J Mater Res Technol 2018, http://dx.doi.org/10.1016/j.jmrt.2008.07.004.
[23] Rietveld HM. A profile refinement method for nuclear and magnetic structures. J Appl Crystallogr 1969;2:65–71.
[24] Lutterotti L. Total pattern fitting for the combined size–strain–stress–texture determination in thin film diffraction. Nucl Instr Methods Phys Res B 2010;268(3–4):334–40.
[25] Brand RA. WinNormos for igor; 2010 http://www.wissel-gmbh.de.
[26] Ramos CP, Sztrajman A, Bianchi R, Danón CA, Saragovi C. Mössbauer spectroscopy analysis on a tempered martensitic 9%Cr steel. Hyperf Interact 2010;195(1):257–63.
[27] Oh SJ, Kwon SJ, Oh H, Lee S, Hwang KC. Phase analysis of two steel work rolls using Mössbauer spectroscopy. Metallur Mater Trans A 2000;31:793–8.
[28] Greenwood NN, Gibb TC. Mössbauer spectroscopy. Chapman and Hall Ltd.; 2012. p. 90.
[29] Wertheim GK, Jaccarino V, Wernick JH, Buchanan DNE. Range of the exchange interaction in iron alloys. Phys Rev Lett 1964;12(1):24–7.
[30] Principi G, Frattini R, Magrini M. Mössbauer analysis of carbides extracted from heat-treated alloy-steels. Gazzetta Chim Ital 1983;113:281–4.
[31] Liu XW, Zhao S, Meng Y, Peng Q, Dearden AK, Huo CF, et al. Mössbauer spectroscopy of iron carbides: from prediction to experimental confirmation. Scient Rep 2016;6: 2618–24.
[32] Schaaf P, Wiesen S, Gonser U. Mössbauer study of iron carbides: cementite $(Fe, M)_3C$ (M = Cr Mn) with various manganese and chromium contents. Acta Metallur Mater 1992;40(2):373–9.
[33] Yang HS, Bhadeshia HKDH. Uncertainties in dilatometric determination of martensite start temperature. Mater Sci Technol 2007;23:556–60.
[34] Jacques PJ, Ladriére J, Delannay F. On the influence of interactions between phases on the mechanical stability of retained austenite in transformation-induced plasticity multiphase steels. Metallurg Mater Trans A 2001;32:2759–68.
[35] Hidalgo J, Findley KO, Santofimia MJ. Thermal and mechanical stability of retained austenite surrounded by martensite with different degrees of tempering. Mater Sci Eng A 2017;690:337–47.
[36] Lančok A, Kmječ T, Štefánik M, Sklenka L, Miglierini M. Structural characterization of highly corrosion-resistant steel. Croat Chem Acta 2015;88:355–61.
[37] Mercader RC, Desimoni J. Mössbauer studies of phase transformations in iron alloys. Hyperf Interact 1997;110:101–9.
[38] Butler B, Cohen J. The location of interstitial carbon in austenite. J Phys I 1992;2(6):1059–65.
[39] Moon KA. Thermodynamics of interstitial solid solutions with repulsive solute–solute interactions. Trans Am Inst of Mining Metallur Petrol Eng 1963:2271–3116.
[40] de Cristofaro N, Kaplow R. Interstitial atom configurations in stable and metastable Fe–N and Fe–C solid solutions. Metallur Trans A 1977;8:35–44.
[41] Brachet J. Correlation between thermoelectric power (TEP) and martensite start temperature (Ms) measurements of 9Cr–W–V–(Ta) martensitic steels. J Phys IV 1995;05(C8):C8-339. C8–344.
[42] Andrews KW. Empirical formulae for calculation of some transformation temperatures. J Iron Steel Inst 1965;203:721–7.
[43] Finkler H, Schirra M. Transformation behaviour of the high temperature martensitic steels with 8–14% chromium. Steel Res 1996;67:328–42.
[44] Suh DW, Han HN, Kim SJ. Plastic strain due to isothermal transformation form austenite to ferrite in IF and low carbon steels. Mater Trans JIM 2007;48:882–5.
[45] Xu PG, Tomota Y, Vogel SC, Suzuki T, Yonemura M, Kamiyama T. Transformation strain and texture evolution during diffusional phase transformation of low alloy steels studied by neutron diffraction. Rev Adv Mater Sci 2013;33:389–95.